arXiv:1411.0188v2 [cond-mat.quant-gas] 1 Jan 2015

Dynamics of shock waves in a superfluid unitary Fermi gas

Wen Wen,[1,*] Tiankun Shui,[2] Yafei Shan,[2] and Changping Zhu[3]

[1]*Department of Mathematics and Physics, Hohai University, Changzhou 213022, China*

[2]*College of Mechanical and Electronic Engineering, Hohai University, Changzhou 213022, China*

[3]*Jiangsu Key Laboratory of Power Transmission and Distribution Equipment Technology, Changzhou Key Laboratory of Sensor Networks and Environmental Sensing, Hohai University, Changzhou 213022, China*

Abstract

We study the formation and dynamics of shock waves initiated by a repulsive potential in a superfluid unitary Fermi gas by using the order-parameter equation. In the theoretical framework, the regularization process of shock waves mediated by the quantum pressure term is purely dispersive. Our results show good agreement with the experiment of Joseph *et al.* [Phys. Rev. Lett. **106**, 150401 (2011)]. We reveal that the boxlike-shaped density peak observed in the experiment consists of many vortex rings due to the transverse instability of the dispersive shock wave. In addition, we study the transition from a sound wave to subsonic shock waves by increasing the strength of the repulsive potential and show a strong qualitative change in the propagation speed of the wavefronts. In the relatively small strength regime, the speed decreases below the sound speed with increasing the strength as a scaling behavior, while in the large regime the speed remains almost unchanged, which is found to be the same expansion speed of the proliferation of the vortex rings.

PACS numbers: 03.75.Kk, 03.75.Lm, 03.75.Ss

*Electronic address: wenwen0emma@163.com

I. INTRODUCTION

The unitary Fermi gas is a system of fermions with an infinite two-body scattering length, which has remarkable universal properties and has connections with areas as diverse as nuclear physics and high-T_c superconductivity [1]. The unprecedented experimental sophistication reached recently in the unitary Fermi gas has opened a unique opportunity for systematic studies of elementary excitations in a strongly interacting Fermi system [2, 3]. Experiments have observed collective modes [4–6] and sound waves [7, 8], nonlinear topological structures including vortices [9] and dark solitons [10, 11], and another specific nonlinear phenomenon, i.e. shock waves [12]. Shock wave generated in a classical fluid is characterized by a well-defined shock front across which, there is a dissipation from the effect of viscosity to avoid the onset of a gradient catastrophe [13, 14]. In contrast to viscous shock wave, shock wave in a Bose-Einstein condensate is mediated by dispersion. Such dispersive shock wave associated with a fast oscillating wave-train trailing has been predicted theoretically [15–19], and then observed in various experiments [20–22].

In the recent experiment performed by the Thomas's group [12], the formation and propagation of shock waves in a unitary Fermi gas were studied by colliding between two clouds. They reproduced the experimental data well by hydrodynamic equations with a phenomenological viscosity term. On the other hand, Bulgac *et al.* [23] and Salasnich *et al.* [24–27] independently argued that the observed fermionic shock front is dominated not by dissipation but rather dispersion, because at zero temperature the bulk viscosity vanishes [28, 29] and the shear viscosity is at a minimum [29, 30]. Since the structures of shock wave fronts are too fine to be imaged in the typical Fermi gas experiments, the regularization mechanism is difficult to be directly revealed through density measurements. In order to determine the appropriate regularization mechanism, Lowman and Hoefer [31] subsequently proposed to measure the propagating speed of shock waves which is regularization dependence [19]. It is noticed that the above mentioned references [24–27, 31] mainly present the results of one dimensional (1D) dynamics of fermonic shock waves by integrating over the transverse coordinate. There is a lack of discussion on the transversal effect on shock wave dynamics, however, which is always present in Fermi gas experiments and of considerable practical interest.

In this work, we use the order-parameter equation to perform a detailed three-dimensional

(3D) numerical simulation of all stages in the experiment of fermionic shock waves [12] and compare to experiment with good agreement. We find that a dispersive shock wave forms, which possess an expanding oscillatory wavetrain with a large amplitude. Due to the transverse instability, the wavetrain decays into a large number of vortex rings in a short time. We interpret that the observed boxlike-shaped density peak in the experiment actually originates from the proliferation of the vortex rings. Furthermore, we study the mechanism of transition from sound wave propagation to shock wave dynamics and present how the wavefront speed depends on the strength of the repulsive potential which creates it. For the smallest strength creating a linear wave, the propagation speed is in good agreement with the theoretically predicted sound speed. As increasing the strength in the relatively weak regime, we find that the speed decreases below the sound speed. In this regime we derive an analytical expression for the speed as a function of the strength from an effective 1D model, which is also confirmed by the full 3D numerical simulation exactly. As the strength increases towards the moderate value, the transversal dynamics takes an effect on the properties of shock waves, and the speed deviates the scaling behavior predicted by the 1D model. As increasing the strength in the sufficiently large regime, shock waves are formed by colliding two spatially separated clouds, and the propagation speeds of the wavefronts are found to be unchanged. We understand the speed independent on the strength as the expansion speed of the vortex rings, which are originated from the decay of the dispersive shock waves due to the transverse instability.

This paper is organized as follows: In Sec. II, we solve numerically the order-parameter equation to study the formation and dynamics of fermionic shock waves in the realistic system. In Sec. III, we analytically and numerically study the transition from sound wave propagation to subsonic shock wave dynamics by calculating the propagation speeds of the wavefronts. Last section gives a conclusion.

II. COMPARISON WITH EXPERIMENT

A. Theoretical description

We consider an ultracold Fermi gas at zero temperature, in which fermionic atoms have two spin states with equal number and all atoms are paired in the superfluid state. The

dynamic behaviors of Fermi superfluids can be described by the following time dependent order-parameter equation [32–36]

$$i\hbar\frac{\partial\Psi_s}{\partial t}=\left[-\frac{\hbar^2\nabla^2}{4m}+2V_{\rm ext}(\mathbf{r})+2\mu(n)\right]\Psi_s, \tag{1}$$

where Ψ_s is the order parameter of fermionic atomic pairs in the condensed state and the atomic density is given by $n=2|\Psi_s|^2$, m is the mass of atom, and $V_{\rm ext}(\mathbf{r})$ is the external potential. In the unitary limit the s-wave scattering length becomes infinity and no characteristic length is set, so the equation of state has the form [37, 38]

$$\mu(n)=\xi\frac{\hbar^2}{2m}(3\pi^2)^{2/3}n^{2/3}, \tag{2}$$

where the Bertsch parameter $\xi=0.38$ is tuned to fit the experimental results [39, 40].

This complex order parameter can be specified by $\Psi_s=\sqrt{\frac{n}{2}}e^{i\Phi_s}$, where Φ_s is the phase of fermionic pair condensates. By introducing the superfluid velocity given by the gradient of the phase $\mathbf{v}=(\hbar/2m)\nabla\Phi_s$, from the order-parameter equation one can deduce the quantum hydrodynamics equations

$$\frac{\partial n}{\partial t}+\nabla\cdot(n\mathbf{v})=0, \tag{3a}$$

$$m\frac{\partial\mathbf{v}}{\partial t}+\nabla\left[\frac{1}{2}mv^2+\mu(n)+V_{\rm ext}(\mathbf{r})-\frac{1}{4}\frac{\hbar^2}{2m}\frac{\nabla^2\sqrt{n}}{\sqrt{n}}\right]=0, \tag{3b}$$

which includes a gradient correction of von-Weizsäcker energy form [41–43] (i.e. quantum pressure term)

$$\lambda\frac{\hbar^2}{2m}\frac{\nabla^2\sqrt{n}}{\sqrt{n}} \tag{4}$$

with $\lambda=1/4$. In absence of the quantum pressure term, Eqs.(3) reduce to the classical hydrodynamic equations [14, 44].

In order to prevent the density gradient catastrophe and model the shock wave formation, Ref. [12] introduces a dissipative viscosity term $\nu\partial_z(n\partial_z v)/n$ into the normalized 1D form of the classical hydrodynamic equations, where $\nu=10\hbar/m$ is fitted to the experimental results. However, it is shown that Fermi gases in the unitary regime have a vanishing viscosity at zero temperature [28–30]. For the quantum hydrodynamics equations (3), an alternative regularization mechanism can be naturally proposed, without the phenomenological viscosity term. The gradient term (4) that takes into account corrections to the kinetic energy due to spatial variations in the density of the system, plays a role of a pure dispersive effect for

the formation of shock waves. There has been a lot of discussion about the value of the coefficient λ [34, 43, 45]. The quantum pressure term depending explicitly on the reduced Planck constant $\hbar$ gives quantization condition, and the value of λ has profound consequences on dynamics of superfluid unitary Fermi gases [24, 26, 27].

Our calculations are based on the order-parameter equation, which models only the dynamics of superfluid components. To further include the mechanism for superfluid relaxation, such as pair-breaking, superfluid-normal transition, and various photon processes, one must resort to time-dependent density functional theory (DFT) which provides a microscopic description [46, 47]. Recently based on DFT, many different dynamical processes have been investigated, including formations of vortex lattices by stirring [47], crossing and reconnection of two vortex lines [47], dynamics of shock waves [23], oscillations of a vortex ring [48], and conversion between vortex rings and vortex lines due to a breaking of the axial symmetry of traps [49], some of which can not be obtained from the order-parameter equation. While the order-parameter equation fails to model the pair-breaking mechanism and normal components, the order-parameter equation depending on a single collective wave function is significantly easier to solve analytically and numerically than DFT, which requires to solve hundreds of thousands of wavefunctions by means of supercomputing resources. In addition, Forbes and Sharma [50] have presented a comparison between the dynamics of superfluid unitary Fermi gases using DFT and the order-parameter equation (they call the extended Thomas-Fermi model), and demonstrated that the order-parameter equation is a good description for low-frequency dynamics of unitary Fermi gases.

B. Numerical results

We solve the order-parameter equation numerically [51] to reproduce as closely as possible the experimental condition. The experimental procedure including three steps is described as follows [12] : (1) The unitary Fermi gas containing a total of $N = 2 \times 10^5$ atoms is initially confined in a cigar-shaped harmonic trap $V_{\rm ho}(\mathbf{r}) = \frac{1}{2}m[\omega_\perp^2(x^2+y^2)+\omega_z^2 z^2]$ with $\omega_\perp = 2\pi \times 437$ Hz and $\omega_z = 2\pi \times 27.7$ Hz, and bisected by a repulsive potential $V_{\rm rep}(z) = V_0 \exp\left[-(z-z_0)^2/\sigma_z^2\right]$ with strength $V_0 = 12.7\ \mu K$, width $\sigma_z = 21.2\ \mu$m and offset $z_0 = -5\ \mu$m. (2) The repulsive potential $V_{\rm rep}$ is then suddenly turned off, allowing for the two separated parts of the cloud to collide with each other in the harmonic trap for a given hold

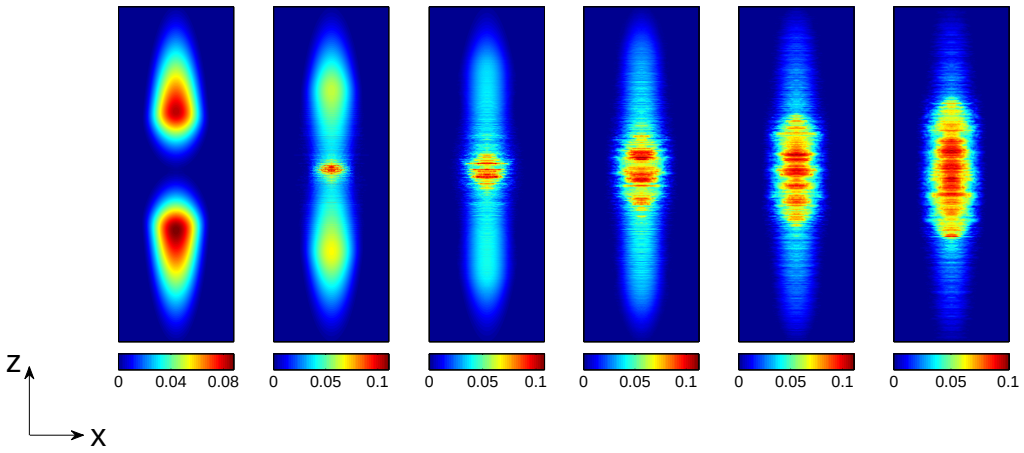


FIG. 1: (Color online) Integrated atomic density profiles (in units of $10^{-3}/\mu m^2$ per particle) after expansion for 1.5 ms after evolving in the trap for different times: from left to right $t = 0$ ms, 2 ms, 4 ms, 6 ms, 8 ms, and 10 ms. Here x and z correspond to the coordinates in μm, with $x \in (-100, 100)$ and $z \in (-210, 210)$.

time t. (3) The absorption images are finally taken after an additional 1.5 ms expansion, during which the harmonic potential in the r-direction is extinguished and the z-direction frequency is changed to $\omega_z = 2\pi \times 20.4$ Hz.

The creation of initial density perturbations undergoing shock wave dynamics achieved experimentally can be classified into two ways [16, 20, 22, 25]: suddenly turning off a repulsive potential produces a dip in the density, which splits into two negative perturbations propagating in opposite directions; alternatively, raising suddenly a repulsive potential results in a density bump, which splits into two positive perturbations. Due to the density-dependent speed that is regions of high density move with a faster local velocity than regions of low density, as they travel the steepenings of leading edges of positive density waves and of trailing edges of negative ones are apparent. Therefore, according to the experimental condition, two negative wave packets propagating in opposite directions are actually observed.

In Figure 1, we show the numerical results for column atomic densities $\int dy\ n(x, y, z, t)$ by integrating along the y axis at different hold times t. It is seen that the presence of the repulsive potential leads to two clearly separated parts. After the potential is rapidly turned off, the two clouds expand and collide at the center of the trap, and a pronounced bulge of higher atom density forms. As the density bulge spreads out from the center of the

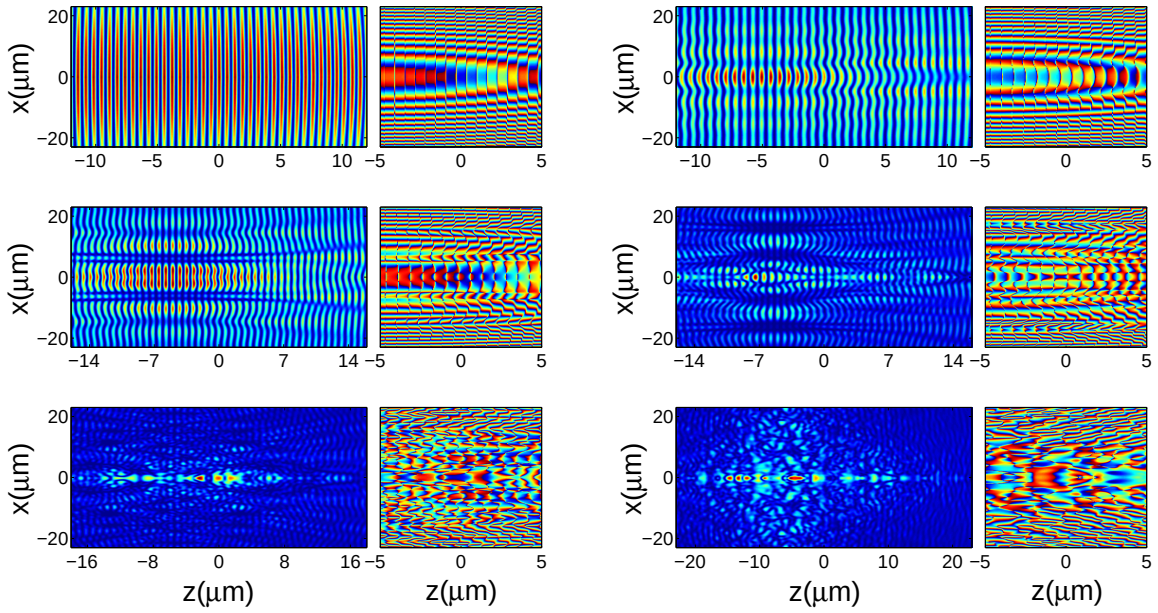


FIG. 2: (Color online) Closeup of the atomic density slices $n(x, 0, z)$ (left panels) and the corresponding phase profiles $\Phi_s(x, 0, z)$ (right panels) after expansion for 1.5 ms after evolving in the trap for different times, from top left to bottom right: $t = 0.7$ ms, 1.1 ms, 1.2 ms, 1.3 ms, 1.5 ms and 2.0 ms. The color corresponds to the phase: $\Phi_s = 0$ through 2π is represented by the sequence blue-green-red-blue.

trap, its front (back) edge self-steepens, which can be identified as the formation of a shock wave. Notice that the observed front and back edges actually correspond to the trailing edges of two negative waves propagating in opposite directions, respectively. The result on the feature of the box-like structure is found to be in good agreement with the experimental observation [see Fig. 1 of Ref. [12]]. However, clear soliton trains in the wake of the density bulge which are indication of the dispersive mechanism are not been found, as that in the experiment.

To better visualize the complicated density distributions at the center of the system and find the dispersive effect, in Figure 2 we present zoomed-in views for the atomic density slices by the plane $y = 0$, that is $n(x, y = 0, z, t)$, and the corresponding phase profiles $\Phi_s(x, 0, z)$. A closer look to the center region reveals that a soliton train forms after evolving in the trap at $t = 0.7$ ms. Subsequently the soliton train is curved as it develops. The curving structure is not symmetric about the $z = 0$ axis, due to the offset $z_0 = -5$ μm of the initial repulsive potential. When $t = 1.3$ ms, the transverse instability causes the quick decay of

the soliton train into the nucleation of vortex rings [48, 52–56], evidenced by the phase profiles. After 2.0 ms, a large number of vortex rings spread over the entire extent of the system. The formation of vortex rings in an initial short time is shown to be difficult to detect unambiguously in the experiment that are integrated along the line of sight [12, 20]. While the phenomena are similar to those found in atomic condensates [20], they are first revealed in a superfluid unitary Fermi gas. Recently based on DFT [23], Bulgac *et al.* studied the shock wave formed in the unitary Fermi gases trapped by a two-dimensional harmonic potential. Because the particle number of the calculated system is too small, no transverse instability is found and the dynamics is characterized by the formation of a soliton train that eventually fills the entire superfluid. Our numerical simulation can be consistent with this (not shown here) if we use small number particle.

III. TRANSITION FROM A SOUND WAVE TO SUBSONIC SHOCK WAVES

Now we study the mechanism of the transition from sound wave propagation to shock wave dynamics by increasing the strength of the repulsive potential and calculate the propagation speeds of the wavefronts. Before presenting the results from a full 3D numerical calculation, we reduce Eqs. (3) into an effective 1D model, derive an analytical solution for the propagating speed that is only valid for small perturbations, and make a comparison with the numerical results.

A. Analytical derivation

We consider a cylindrically symmetric external potential composed of the harmonic potential in the transverse direction and an axial potential: $V_{\rm ext}(\mathbf{r},t) = \frac{1}{2}m\omega_\perp^2 r^2 + V_1(z,t)$, with $r = \sqrt{x^2+y^2}$. The atomic density and superfluid velocity are then expressed as [31]

$$n(\mathbf{r},t) = n_\perp[r; n_1(z,t)]n_1(z,t) \quad \text{and} \quad \mathbf{v}(\mathbf{r},t) = v_1(z,t). \tag{5}$$

The atomic density satisfies the normalization conditions: $2\pi\int dr\, r n_\perp = 1$ and $\int dz n_1 = N$. We assume sufficiently tight transverse confinement so that its dynamics is neglected. Under the Thomas-Fermi (TF) approximation, the density distribution in the equilibrium is given

by

$$n_\perp[r;n_1] = n_\perp(0)(1-\frac{r^2}{R_\perp^2})^{3/2}, \qquad R_\perp^2 = \frac{2\mu_\perp}{m\omega_\perp^2}. \tag{6}$$

By the normalization condition $2\pi\int_0^{R_\perp} drrn_\perp$=1, the center atomic density and chemical potential are then given by

$$n_\perp(0) = (\frac{2m\mu_\perp}{\xi\hbar^2})^{3/2}(6\pi^2 n_1)^{-1}, \quad \mu_\perp = \bar{\mu}n_1^{2/5} = (\frac{15\pi m\omega_\perp^2}{4})^{2/5}(\frac{\xi\hbar^2}{2m})^{3/5}n_1^{2/5}, \tag{7}$$

respectively. Substituting the above ansatz into Eqs. (3) and integrating over the transverse coordinate, one can arrive at the effective 1D hydrodynamic equations

$$\frac{\partial n_1}{\partial t} + \frac{\partial}{\partial z}(n_1 v_1) = 0, \tag{8a}$$

$$m\frac{\partial v_z}{\partial t} + \frac{\partial}{\partial z}\left[\frac{1}{2}mv_z^2 + \bar{\mu}n_1^{\frac{2}{5}} + V_1\right] = 0, \tag{8b}$$

with $\bar{\mu}$ defined in Eq. (7). Notice that the power of the nonlinear term for the density has changed from 2/3 to 2/5 as we pass from the 3D decription Eqs. (3) to the effective 1D model Eqs. (8). In additon, we assume that the spatial scale of the density perturbation is larger than the healing length and neglect the gradient correction (i.e. quantum pressure) term.

In the case of the axial harmonic potential $V_1 = \frac{1}{2}m\omega_z^2 z^2$, one has the ground-state solution of Eq. (8b)

$$n_1(z) = n_1(0)(1-\frac{z^2}{R_z^2})^{5/2}, \quad R_z^2 = \frac{2\mu_G}{m\omega_z^2}, \tag{9}$$

where μ_G is the ground-state chemical potential fixed by the normalized condition $\int_{-R_z}^{R_z} dzn_1 = N$. It is easy to get the explicit expressions

$$n_1(0) = (\mu_G/\bar{\mu})^{5/2}, \qquad \mu_G = \sqrt{\xi}E_F, \tag{10}$$

with the Fermi energy $E_F = \hbar(3N\omega_\perp^2\omega_z)^{1/3}$. After linearization of Eqs. (8), one can obtain the local speed of sound calculated at the center of the trap [57, 58]

$$c_s^2 = \frac{2\bar{\mu}}{5m}n_1^{2/5}(0) = \frac{1}{5}\xi^{\frac{1}{2}}v_F^2 \tag{11}$$

with the Fermi velocity $v_F = \sqrt{2E_F/m}$. We find that such local sound speed $c_s = \sqrt{\xi^{1/2}/5}v_F$ is smaller than the sound speed $c_{\rm ho} = \sqrt{\xi/3}v_F$ of a homogeneous system [59] by a factor of $\sqrt{3/5\xi^{1/2}} = 0.987$, which is resulted from the suppression of the transverse confinement.

We perform the ansatz on the density $n_1(z,t) = n_1(0)\rho(z,t)$, which implies a homogenous density background characterized by the central density. By substituting it and Eq. (11) into Eqs. (8), the effective 1D hydrodynamic equations are written as

$$\frac{\partial \rho}{\partial t} + \rho\frac{\partial v_z}{\partial z} + v_z\frac{\partial \rho}{\partial z} = 0, \tag{12a}$$

$$\frac{\partial v_z}{\partial t} + v_z\frac{\partial v_z}{\partial z} + \frac{c_{ls}^2}{\rho}\frac{\partial \rho}{\partial z} = 0, \tag{12b}$$

with

$$c_{ls}(\rho) = c_s\rho^{\frac{1}{5}}. \tag{13}$$

In order to find wave solutions of Eqs. (12), it is assumed that the velocity v_z depends explicitly the density ρ [25]. In this case one can put $\partial v_z/\partial t = \frac{dv_z}{d\rho}\frac{\partial \rho}{\partial t}$, $\partial v_z/\partial z = \frac{dv_z}{d\rho}\frac{\partial \rho}{\partial z}$, and reduce Eqs. (12) to a hyperbolic equation

$$\frac{\partial \rho}{\partial t} + C(\rho)\frac{\partial \rho}{\partial z} = 0. \tag{14}$$

It is easy to find the exact traveling wave solution of the hyperbolic equation: $\rho = f(z, C(\rho(z,t))t)$, where f is an arbitrary function and $C(\rho) = v_z + c_{ls}^2(dv_z/d\rho)^{-1}/\rho$ is the local speed of propagation. By a requirement that far from the perturbation the density is equal to one and the velocity field is zero, the local speed is then given as $C(\rho) = \pm c_s(6\rho^{1/5} - 5)$, where the sign $\pm$ determines a direction of propagation. The repulsive potential produces an initial density $\rho(z,0) = (1 + A\exp(-z^2/\sigma^2))^{5/2}$, where the magnitude of A is proportional to the strength, i.e. $|A| \propto V_0$. After the repulsive potential is suddenly turned off or switched on, the Gaussion shaped perturbation breaks into two separate parts with half-amplitude of the initial perturbation moving in the opposite directions [16, 25, 60]. The extrema of the traveling wave has a constant amplitude $1 + \eta$, and its speed is given by

$$c(\eta) = c_s[6(1+\eta)^{1/5} - 5], \tag{15}$$

where the wave amplitude is determined by the strength of the repulsive potential through the relation $\eta = [(1 + A)^{5/2} - 1]/2$ [60]. It is seen that the speed of shock waves explicitly depends on initial conditions. In the limit $A \sim 0$, the speed reduces to the sound speed c_s. For $A < 0$ ($A > 0$) corresponding to negative (positive) perturbations, one has subsonic (supersonic) waves.

In the above analytical discussion, we assumed that the transverse density is approximated by the TF ground-state, which means that the dynamics in the transverse direction

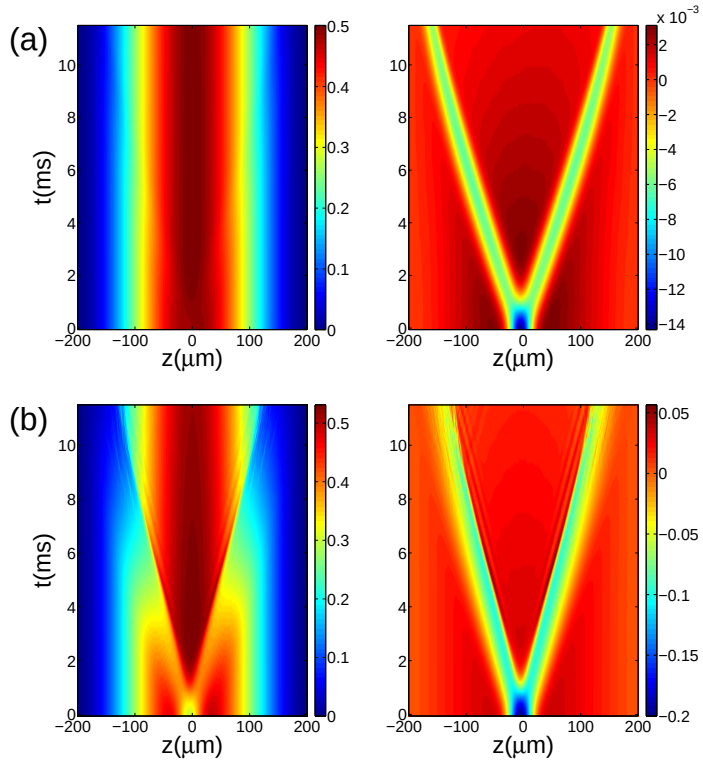


FIG. 3: (Color online) Space-time evolutions in the harmonic trap of the atomic density for relatively weak repulsive potential strengthes $|A| = V_0/\mu_G$ with the chemical potential $\mu_G = 0.435\mu K$. The atomic density integrated along the transverse direction is in units of $10^{-2}/\mu m$ per particle. Panels (a) and (b) correspond to $|A| = 0.0153$ and 0.23, respectively. Left: the actual density. Right: the normalized density (the actual density minus the ground-state density).

is frozen and no instability occurs as studied in Refs. [16, 25, 31]. Salasnich obtained the propagation speed of the shock waves proportional to $[4(1+\eta)^{1/3} - 3]$ in a different configuration [25], i.e. 3D homogenous unitary Fermi gas. Such expression differs from our result only for the constants, because the integration of the transversal harmonic confinement leads the power of the nonlinear term to change from 2/3 to 2/5. Therefore, one can predict the speed of the shock waves in a homogeneous BEC in proportion to $[3(1+\eta)^{1/2} - 2]$ [16], due to the nonlinear power 2/2. Based on the effective 1D hydrodynamic equations (8) incorporating the quantum pressure term (4), Lowman and Hoefer obtained implicit relations for the speeds of supersonic shock waves [31]. However, numerical simulation in the following will show that the analytical result is only valid for relatively weak repulsive potentials. As the strength of the potential increases, the dispersive shock wave is created with larger ampli-

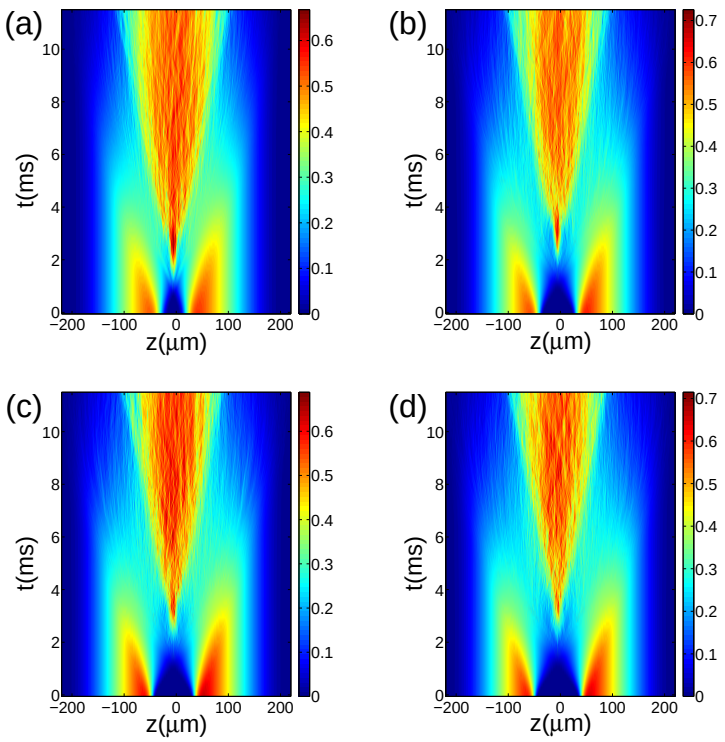


FIG. 4: (Color online) Space-time evolutions in the harmonic trap of the atomic density for repulsive potential strengthes $|A| > 1$. The atomic density integrated along the transverse direction is in units of $10^{-2}/\mu m$ per particle. Panels (a), (b) and (c) correspond to $|A| = 1.22$, 6.11, and 14.6, respectively. Panel (d) shows the experimental case $|A| = 29.2$.

tude of oscillating wave-trains. In a strongly interacting Fermi gas, they are easily subject to the transverse instability that leads to the formation of vortex rings [48, 52–54]. Such decay process eventually takes an significant effect on the dynamical properties of shock waves.

B. numerical results

In the following we numerically solve the order-parameter equation to study the formation and dynamics of shock waves in the harmonic trap, which are initiated by different strengthes of the repulsive potential under the experimental conditions. Due to the perturbations are created by suddenly turning off the repulsive potential, they are negative and subsonic. The amplitude of the perturbation is then expressed by $\eta = [(1 - |A|)^{5/2} - 1]/2$, where the magnitude $|A| = V_0/\mu_G$ is characterized by the ratio of strength of the repulsive potential to chemical potential, and $\mu_G = 0.435\ \mu K$ is obtained by substituting the experimental

parameters into Eq. (10).

Figure 3 shows the space-time evolutions of the atomic density integrated along the transverse direction at relatively small repulsive potential strengthes, and other parameters are the same as the experimental parameters. Fig. 3(a) shows the case of a very small perturbation $|A| = 0.0153$. However, in the left panel the propagation of the wave cannot be directly observed through the density profile. In order to visualize the trajectory of the wave, we present the normalized density profile in the right panel, i.e. the actual density subtracts the ground-state density. It is clear that the initially induced negative perturbation splits into two density dips, which propagate outward at an almost constant speed and slow down when approaching the superfluid boundary due to the density dependence of the speed. For such weak perturbation $|A| \sim 0$, one might expect to excite linear wave. One can extract the propagation speed from the center of the normalized density profile [7, 8]. The obtained speed of $0.347v_F$ is consistent with the analytical prediction $c_s = \sqrt{\xi^{1/2}/5}v_F = 0.351v_F$. With increasing $|A| = 0.23$ in Fig. 3(b), in the left panel we observe directly the formation of the shock wave from the density profile, in which the shock front is represented as a sharp discontinuity of the two density lines forming a "V" shape. In addition, one can see that after a long time dynamics, the steepness of the shock wave front is associated with oscillatory behaviors, which are more obvious from the normalized density profile in the right panel.

In Figure 4, we show the space-time evolutions of the atomic density initiated by large potential strengthes $|A| > 1$, which means that the repulsive potential results in two spatially separated clouds. Fig. 4(a) corresponds to the case of $|A| = 1.22$. Different from the cases of initial small perturbations in Fig. 3, the density oscillation behaivors begin to occur in the overlap of the two clouds at the center of the system. For larger values of the strengthes in Fig. 4(b) ($|A| = 6.11$) and Fig. 4(c) ($|A| = 14.6$), stronger oscillations of the densities in more extensive regions are observed. But interestingly, from panels (a) to (d) we notice that the simulations present very similar characteristic of the "V" shape. Fig. 4(d) shows the experimental situation $|A| = 29.2$, which is in agreement with the experimental results [see Fig. 1 of Ref. [23]]. Noticed that compared to the experimental observation in Fig. 1 of Ref. [23], which is on an expanded scale realized by an additional 1.5 ms expansion after evolving in the harmonic trap (i.e. all three steps described in Sec. IIB are included), in Fig. 3 and 4 we present the space-time evolutions in the harmonic trap without the additional expansion

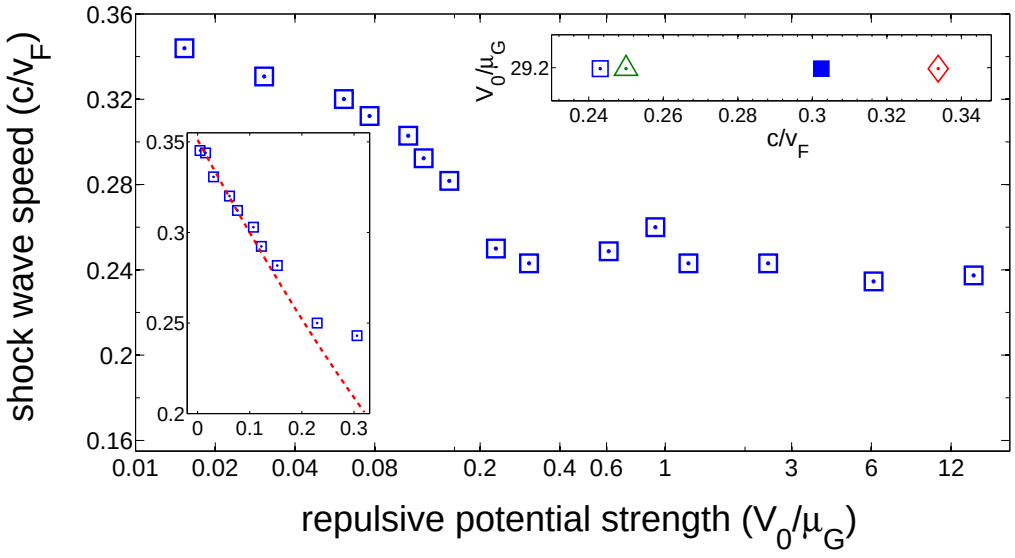


FIG. 5: (Color online) Propagation speed of the shock wave fronts as a function of the strength of the repulsive potential. Left insert: the comparison of the numerical simulations (□) and the analytical prediction Eq.(15) (dashed line). Right inset: the comparison of the results of the experiment (♢) [12], the density functional theory (△) [23], and our results calculated for the cases in the harmonic trap (□) and after an additional expansion (filled □).

(i.e. only the first two steps are included).

From Fig. 3 and 4 we not only observe the transition from a sound wave to shock waves, but we also extract the propagation speeds of the shock wave fronts by calculating the slopes of the two lines in the "V" shape. The propagation speed of the shock waves as a function of the repulsive potential strength is plotted in Figure 5. Two approximate regimes can be distinguished: In the relatively small strength regime, the propagation speed decreases below the sound speed as the strength increases. In the left inset we compare the numerical results (□) to the analytical prediction Eq. (15) (dashed line). One can find that the analytical expression agrees very well with the numerical results in the very small strength regime ($|A| < 0.2$). In this regime, the transversal dynamics has a negligible effect, so that Eq. (15) is an accurate expression for the speed of the shock waves derived from the effective 1D model. Specifically, one can see that for $|A| > 0.3$ the speed presents a significant deviation from the analytical prediction, which indicates that the 1D model is not adequate in the description of the 3D system. The other interesting regime is $|A| > 1$ corresponding to the cases of Fig. 4, we find the propagation speed of the wavefront is independent on the value

of the strength, and remains about $0.24v_F$. The physical reason for the unchanged speed can be explained as follows. For the regime of $|A| > 1$, the shock wave is formed by colliding two initial separated clouds. As these two clouds are close each other and overlap gradually at the center of the trap, the dispersive effect results in the formation of soliton trains. Due to the transverse instability, the soliton trains quickly decay into vortex rings and the density bulge peak is formed by filling with the numerous vortex rings. We calculated the propagation speed of the shock waves from the movements of self-steepen edges of the bulge peak. Therefore, the obtained speeds actually correspond to the same expansion speed of the proliferation of the vortex rings.

In the right inset, we show the numerical results for the experimental situation $|A| = 29.2$ calculated from two different situations. One denoted by open square is obtained from the density profiles after evolving in the harmonic trap (see Fig. 4(d)), while the other by filled square is calculated from the density profiles after expansion for 1.5 ms after evolving in the harmonic trap as performed in the experiment (see Fig. 1). The speed of $0.302v_F$ obtained from the profiles after the additional expansion is much larger than $0.243v_F$ calculated in the trap. This is because such expansion method enhances the difference of the wavefront positions at two sequence times. The result ($0.25v_F$, triangle) based on the DFT [23] and the experimental data ($0.33v_F$, diamond) [12] are also shown for comparison.

IV. CONCLUSION

In conclusion, based on the order-parameter equation we have presented a detailed study for the experiment on dynamics of shock waves in the unitary superfluid Fermi gas performed by the Thomas's group, which shows good agreement with the experiment. The shock wave is studied by colliding two spatially separated clouds. As the two clouds gradually overlap at the center of the trap, a soliton train forms due to the dispersive effect provided by the quantum pressure term. Due to the transverse instability, the soliton train decays very quickly into a large number of vortex rings. The boxlike-shaped density peak observed in the experiment is then interpreted by the proliferation of the vortex rings. In addition, we have studied the mechanism of transition from a sound wave to shock waves by calculating the speeds of the wavefronts and given an explanation why the speed of the shock wave observed in the experiment is so close to the sound speed. For a very small strength of the initial

repulsive potential, sound wave is created with the propagation speed of $0.347v_F$. As the strength increases in the relatively weak regime, the nonlinear effect leads to the formations of shock waves, and the speed decreases below the sound speed as a scaling behavior. When the strength is moderate, the transversal dynamics takes an effect to suppress the decrease of the speed. For the large strength regime where the shock wave is formed by colliding two separated clouds, the propagation speed of the wavefront is independent on the strength and remains about $0.24v_F$. We understand this speed as the expansion speed of the proliferation of the vortex rings. Finally, our numerical simulation demonstrates that the expansion image method results in calculating the propagation speed from $0.243v_F$ to $0.302v_F$, which is very close to $0.33v_F$ of the experimental observation.

Acknowledgments

We would like to thank John Thomas and James Joseph for suggesting to study the propagation speed of the shock wave fronts, and useful comments on the manuscript. We also thank Han Pu for the critical comments on the manuscript. W.W. thanks the hospitality of KITPC where part of the writing is done, and useful discussions with Hui Zhai. This work is supported by the NSFC under Grant (No. 11105039 and No. 11274092), and Fundamental Research Funds for the Central Universities of China (Program No. 2012B05714 and No. 2014B11414).

---

[1] W. Zwerger, ed., *The BCS-BEC Crossover and the Unitary Fermi Gas*, Lecture Notes in Physics, Vol. 836 (Springer-Verlag, Berlin, 2012).

[2] W. Ketterle and M. W. Zwierlein, *Riv. Nuovo Cimento* **31**, 247 (2008).

[3] A. Adams, L. D. Carr, T. Schäfer, P. Steinberg and J. E. Thomas, New J. Phys. **14**, 115009 (2012).

[4] J. Kinast, S. L. Hemmer, M. E. Gehm, A. Turlapov, and J. E. Thomas, Phys. Rev. Lett. **92**, 150402 (2004).

[5] M. Bartenstein, A. Altmeyer, S. Riedl, S. Jochim, C. Chin, J. H. Denschlag, and R. Grimm, Phys. Rev. Lett. **92**, 203201 (2004); A. Altmeyer, S. Riedl, C. Kohstall, M. J. Wright, R.

Geursen, M. Bartenstein, C. Chin, J. H. Denschlag, and R. Grimm, *ibid.* **98**, 040401 (2007); A. Altmeyer, S. Riedl, M. J. Wright, C. Kohstall, J. H. Denschlag, and R. Grimm, Phys. Rev. A **76**, 033610 (2007).

[6] M. K. Tey, L. A. Sidorenkov, Edmundo R. Sánchez Guajardo, R. Grimm, M. J. H. Ku, M. W. Zwierlein, Y. H. Hou, L. Pitaevskii and S. Stringari, Phys. Rev. Lett. **110**, 055303 (2013).

[7] J. Joseph, B. Clancy, L. Luo, J. Kinast, A. Turlapov, and J. E. Thomas, Phys. Rev. Lett. **98**, 170401 (2007).

[8] L. A. Sidorenkov, M. K. Tey, R. Grimm, Y. -H. Hou, L. Pitaevskii and S. Stringari, Nature **498**, 78 (2013).

[9] M. W. Zwierlein, J. R. Abo-Shaeer, A. Schirotzek, C. H. Schunck, and W. Ketterle, Nature **435**, 1047 (2005).

[10] T. Yefsah, A. T. Sommer, M. J. H. Ku, L. W. Cheuk, W. Ji, W. S. Bakr and M. W. Zwierlein, Nature **499**, 426 (2013).

[11] M. J. H. Ku, W. Ji, B. Mukherjee, E. Guardado-Sanchez, L. W. Cheuk, T. Yefsah, and M. W. Zwierlein, Phys. Rev. Lett. **113**, 065301 (2014).

[12] J. A. Joseph, J. E. Thomas, M. Kulkarni and A. G. Abanov, Phys. Rev. Lett. **106**, 150401 (2011).

[13] G. B. Whitman, *Linear and Nonlinear Waves*, (Wiley, New York, 1974).

[14] L. D. Landau and E. M. Lifshitz, *Fluid Mechanics*, (Pergamon Press, Loundon, 1987).

[15] I. Kulikov and M. Zak, Phys. Rev. A **67**, 063605 (2003).

[16] B. Damski, Phys. Rev. A **69**, 043610 (2004).

[17] A. M. Kamchatnov, A. Gammal, and R. A. Kraenkel, Phys. Rev. A **69**, 063605 (2004).

[18] V. M. Pérez-García, V. V. Konotop, and V. A. Brazhnyi, Phys. Rev. Lett. **92**, 220403 (2004).

[19] M. A. Hoefer, M. J. Ablowitz, I. Coddington, E. A. Cornell, P. Engels, and V. Schweikhard, Phys. Rev. A **74**, 023623 (2006).

[20] J. J. Chang, P. Engels, and M. A. Hoefer, Phys. Rev. Lett. **101**, 170404 (2008).

[21] Z. Dutton, M. Budde, C. Slowe and L. V. Hau, Science **293**, 663 (2001).

[22] R. Meppelink, S. B. Koller, J. M. Vogels, P. van der Straten, E. D. van Ooijen, N. R. Heckenberg, H. Rubinsztein-Dunlop, S. A. Haine and M. J. Davis, Phys. Rev. A **80**, 043606 (2009).

[23] A. Bulgac, Y.-L. Luo, and K. J. Roche, Phys. Rev. Lett. **108**, 150401 (2012).

[24] F. Ancilotto, L. Salasnich, and F. Toigo, Phys. Rev. A **85**, 063612 (2012).

[25] L. Salasnich, Europhys. Lett. **96**, 40007 (2011).

[26] F. Ancilotto, L. Salasnich, and F. Toigo, J. Low Temp. Phys. **171**, 329 (2013).

[27] L. Salasnich, Few-Body Syst. **54**, 697 (2013).

[28] D. T. Son, Phys. Rev. Lett. **98**, 020604 (2007).

[29] C. Cao, E. Elliott, H. Wu and J. E. Thomas, New J. Phys. **13**, 075007 (2011); J. A. Joseph, E. Elliott, and J. E. Thomas, arXiv:1410.4835.

[30] G. Wlazłowski, P. Magierski, and J. E. Drut, Phys. Rev. Lett. **109**, 020406 (2012).

[31] N. K. Lowman and M. A. Hoefer, Phys. Rev. A **88**, 013605 (2013).

[32] L. Salasnich, N. Manini, and F. Toigo, Phys. Rev. A **77**, 043609 (2008).

[33] S. K. Adhikari, Phys. Rev. A **77**, 045602 (2008).

[34] L. Salasnich and F. Toigo, Phys. Rev. A **78**, 053626 (2008).

[35] S. K. Adhikari and L. Salasnich, Phys. Rev. A **78**, 043616 (2008).

[36] W. Wen, Y. Zhou, and G. Huang, Phys. Rev. A **77**, 033623 (2008).

[37] J. Carlson, S.-Y. Chang, V. R. Pandharipande, and K. E. Schmidt, Phys. Rev. Lett. **91**, 050401 (2003).

[38] A. Bulgac, J. E. Drut and P. Magierski, Phys. Rev. Lett. **96**, 090404 (2006).

[39] N. Navon, S. Nascimbène, F. Chevy, and C. Salomon, Science **328**, 729 (2010).

[40] M. J. H. Ku, A. T. Sommer, L. W. Cheuk, and M. W. Zwierlein, Science **335**, 563 (2012).

[41] A. L. Zubarev, J. Phys. B: At. Mol. Opt. Phys. **42**, 011001 (2009).

[42] A. L. Zubarev and M. Zoubarev, Europhys. Lett. **87**, 33001 (2009).

[43] A. Csordás, O. Almásy, and P. Szépfalusy, Phys. Rev. A **82**, 063609 (2010).

[44] C. Menotti, P. Pedri, and S. Stringari, Phys. Rev. Lett. **89**, 250402 (2002).

[45] Y. E. Kim and A. L. Zubarev, Phys. Rev. A **70**, 033612 (2004).

[46] A. Bulgac and M. M. Forbes, in *Quantum Gases: Finite Temperature and Non-Equilibrium Dynamics*, Cold Atoms Series, Vol. 1, edited by N. P. Proukakis *et al.* (Imperial College Press, London, 2013), Chap. 26.

[47] A. Bulgac, Y.-L. Luo, P. Magierski, K. J. Roche, and Y. Yu, Science **332**, 1288 (2011).

[48] A. Bulgac, Michael McNeil Forbes, Michelle M. Kelley, K. J. Roche, and G. Wlazłowski, Phys. Rev. Lett. **112**, 025301 (2014).

[49] G. Wlazłowski, A. Bulgac, M. M. Forbes, and K. J. Roche, arXiv:1404.1038.

[50] Michael McNeil Forbes and R. Sharma, Phys. Rev. A **90**, 043638 (2014).

[51] S. K. Adhikari, J. Phys. B: At. Mol. Opt. Phys. **43**, 085304 (2010).

[52] A. Cetoli, J. Brand, R. G. Scott, F. Dalfovo, and L. P. Pitaevskii, Phys. Rev. A **88**, 043639 (2013).

[53] A. M. Mateo and J. Brand, Phys. Rev. Lett. **113**, 255302 (2014).

[54] W. Wen and H.-J. Li, J. Phys. B: At. Mol. Opt. Phys. **46**, 035302 (2013).

[55] D. L. Feder, M. S. Pindzola, L. A. Collins, B. I. Schneider, and C. W. Clark, Phys. Rev. A **62**, 053606 (2000).

[56] M. A. Hoefer and B. Ilan, Multiscale Model. Simul. **10**, 306 (2012).

[57] P. Capuzzi, P. Vignolo, F. Federici, and M. P. Tosi, Phys. Rev. A **73**, 021603(R) (2006).

[58] W. Wen, S. -Q. Shen and G. Huang, Phys. Rev. B **81**, 014528 (2010).

[59] H. Heiselberg, Phys. Rev. A **73**, 013607 (2006).

[60] B. Damski, J. Phys. B: At. Mol. Opt. Phys. **37**, L85 (2004).